

## Article

# Mechano-Chemical Properties and Tribological Performance of Thin Perfluoropolyether (PFPE) Lubricant Film under Environmental Contaminants

Yeonjin Jung and Changdong Yeo \* 

Department of Mechanical Engineering, Texas Tech University, Lubbock, TX 79409, USA; yeonjin.jung@ttu.edu  
\* Correspondence: changdong.yeo@ttu.edu; Tel.: +1-806-834-5452

**Abstract:** Through molecular dynamics (MD) simulations with ReaxFF potential, the effects of chemical contaminants on the mechano-chemical properties and tribological performance of perfluoropolyether (PFPE) lubricants were investigated. For the two types of contaminants, i.e., silicon dioxide (SiO<sub>2</sub>) nanoparticles and water (H<sub>2</sub>O), their molecular interactions with the two different PFPE lubricants, i.e., Ztetraol and ZTMD, were evaluated at the two different temperatures, i.e., 300 K and 700 K. Contaminants were adsorbed onto the PFPE lubricants at a controlled temperature. Then, air shear simulations were conducted to examine the mechano-chemical behaviors of the contaminated lubricants. Sliding contact simulations were performed to further investigate the tribological performance of the contaminated lubricants, from which the resulting friction and surface contamination were quantified. Lastly, chemical reactions between PFPE lubricants and contaminants were studied to investigate the degradation of PFPE lubricants. It was observed that SiO<sub>2</sub> nanoparticles stiffened the PFPE lubricant, which decreased its shear displacement and increased friction. In the case of the H<sub>2</sub>O contaminant, it weakened and decreased the PFPE lubricant's viscosity, increasing its shear displacement and lowering friction. However, the decreased viscosity by H<sub>2</sub>O contaminants can weaken the lubricity of the PFPE lubricant, leading to a higher chance of direct solid-to-solid contact under high contact force conditions.

**Keywords:** PFPE lubricants; ReaxFF; MD simulation; contaminants



Citation: Jung, Y.; Yeo, C.

Mechano-Chemical Properties and Tribological Performance of Thin Perfluoropolyether (PFPE) Lubricant Film under Environmental Contaminants. *Lubricants* **2023**, *11*, 306. <https://doi.org/10.3390/lubricants11070306>

Received: 21 June 2023

Revised: 13 July 2023

Accepted: 18 July 2023

Published: 21 July 2023



**Copyright:** © 2023 by the authors. Licensee MDPI, Basel, Switzerland. This article is an open access article distributed under the terms and conditions of the Creative Commons Attribution (CC BY) license (<https://creativecommons.org/licenses/by/4.0/>).

## 1. Introduction

In hard disk drives (HDDs), the head-media-spacing (HMS) budget and the magnetic domain size of a recording media are the critical design parameters to increase the data capacity. As the current perpendicular magnetic recording (PMR) technology becomes fully matured and reaches its maximum data capacity limit, new technology is required to make a breakthrough in the areal density of HDDs. One of the promising technologies is heat-assisted magnetic recording (HAMR). Using a metallic optical near-field transducer (NFT), magnetic domains of a recording medium are temporarily heated to its Curie temperature, which reduces its coercivity and accordingly enables it to make a smaller bit [1].

Even though HAMR technology can ensure a much higher areal density than PMR products, it can have critical head-disk-interface (HDI) failures due to the low HMS and elevated material temperature [2]. One fatal and well-known HDI issue in HAMR is the head slider's surface contamination, which worsens under external contaminants inside the HDD [3,4]. Siloxane is a widespread contaminant found inside HDD, which comes from the sealing materials of HDD components. It has been reported that siloxane molecules near the HDI can accumulate on the head or media surface [3] and form silicon dioxide (SiO<sub>2</sub>) as a result of the reaction between lubricants and siloxanes at high temperatures [5]. SiO<sub>2</sub> nanoparticles are often used as lubricant additives to improve tribological properties, such as a reduced coefficient of friction, wear volume, and corrosion [6–10]. However, under a nanocontact condition, such as in a HDD, accumulation in the form of either siloxane

or SiO<sub>2</sub> can increase the head slider's mechanical instability and surface contamination by physical HDI contact, which can cause a critical reading and writing failure due to the low HMS [2–4,11–13]. Another undesirable contaminant in HDI is water molecules, because they are readily adsorbed into the thin perfluoropolyether (PFPE) lubricant on a recording medium. Previous experimental studies showed that hydroxyl endgroups (–OH) in the Fomblin Z-dol lubricant interact with water molecules, which degrades the lubricant properties, producing unstable HDI behaviors at elevated temperatures and humidity conditions [14–20]. Also, from molecular dynamics (MD), it can be observed that the adsorption of silicon dioxide (SiO<sub>2</sub>) nanoparticles into PFPE lubricant can increase the HDI friction force and the lubricant pick-up [21].

Perfluoropolyether (PFPE) has long been used as a lubricant on magnetic recording media in HDDs due to its chemical inertness, low volatility, thermal stability, and superior lubrication properties [20,22,23]. A PFPE lubricant typically comprises a backbone chain and hydroxyl endgroups (–OH). Hydroxyl endgroups are highly polar interactive and act to anchor firmly on the underlying diamond-like-carbon (DLC) film. A backbone chain is made of strong covalent bonds, such as C–O, C–F, C–C, and C–H. It is known that the C–O bond provides flexibility and thermal stability, the C–F bond shows superior chemical resistance and low surface energy, resulting in reduced friction and improved lubricity [24], the C–C bonds form the main carbon backbone, ensuring structural integrity, and the C–H bond allows for interactions with surfaces, supporting lubrication compared to other bonds of the backbone chain [25].

Several PFPE lubricants have been used in HDD products, such as Z-dol, Ztetraol, D-4OH, and Ztetraol multidentate (ZDMD). Researchers have studied low-profile lubricants to achieve a lower HMS and higher areal density for HDDs. For example, ZTMD was synthesized by oligomerizing short Ztetraol and introducing additional functional groups [26]. The additional hydroxyl groups in ZTMD provide stronger chemical affinity, improved shear resistance, and a lower HMS compared with Ztetraol [26,27]. As HAMR technology increases the lubricant temperature up to the Curie temperature of a magnetic recording medium, it may require further advancement of the lubricant design. Researchers have investigated the relationship between PFPE lubricants and high temperatures under HAMR conditions through experiments, material characterization techniques, and computational simulations. An experimental study reported that Ztetraol was the first component to decay, and the lubricant loss amount decreased as the maximum temperature or number of heating cycles increased [28]. Another study predicted the lubricant transfer under the HAMR condition, and it showed that the lubricant transfer mechanism is significantly thermally driven by considering different sizes of the laser spot and disjoining pressure [29]. The use of a high operation temperature for HAMR was studied through MD simulations using D4OH, Ztetraol, Demnum, and Z at operation temperatures of 700 K and 800 K. They found that pure thermal decomposition within a 1 ns heating time rarely happens, and polar PFPE lubricants (i.e., D4OH and Ztetraol) are more likely to decompose than nonpolar PFPE lubricants (i.e., Demnum and Z) [30].

In this study, we investigated the effects of HDI contaminants on the mechano-chemical properties and tribological performance of PFPE lubricants through MD simulations with ReaxFF potential [31]. A comparative study was conducted using two types of contaminants (i.e., SiO<sub>2</sub> and H<sub>2</sub>O) and two different PFPE lubricants (i.e., Ztetraol and ZTMD) at ambient temperature and 700 K.

## 2. Methods

### 2.1. ReaxFF Forcefield

ReaxFF describes atomistic reaction processes by updating the bond order of each iteration and accurately provides bond breaking and formation information in a molecular dynamics (MD) simulation [32].

$$E_{\text{system}} = E_{\text{bond}} + E_{\text{cover}} + E_{\text{under}} + E_{\text{tor}} + E_{\text{val}} + E_{\text{lp}} + E_{\text{vdW}} + E_{\text{coulomb}} \quad (1)$$

The total energy term,  $E_{\text{system}}$ , in Equation (1) is interpreted as the sum of the various energy terms.  $E_{\text{bond}}$ ,  $E_{\text{over}}$ ,  $E_{\text{under}}$ ,  $E_{\text{tor}}$ ,  $E_{\text{val}}$ ,  $E_{\text{lp}}$ ,  $E_{\text{vdW}}$ , and  $E_{\text{coulomb}}$  are the energy terms of the bonds, over-coordination, under-coordination, torsion angle, valence angle, lone pair, van der Waals, and coulombic interaction, respectively [33]. Compared to non-reactive force fields, ReaxFF includes additional concepts, such as the bond order, under-coordination, and over-coordination terms, which ensure adaption to the instantaneous configuration in the reactive system [34]. The applied ReaxFF potential parameter set in this study was developed by Chipara et al. [35], combining C/H/O interactions [32,36], the Si/C interaction [37], and the newly trained C/F interaction [35]. To perform MD simulations, the ReaxFF parameter set was applied in a LAMMPS (Large-scale Atomic/Molecular Massively Parallel Simulator) [38].

## 2.2. Material Preparations and Contaminant Adsorption

### 2.2.1. Lubricant Preparation

Ztetraol and Ztetraol multidentate (ZTMD) were prepared using Materials Studio and Avogadro [39]. Based on previous studies [21,40,41], the chemical structures for Ztetraol and ZTMD were chosen, as shown in Figure 1. Both PFPE lubricants were optimized by using the NWChem computational chemistry package [42] with the B3LYP functional approximation [43], Mulliken population for electronic charge distribution [44], and the STO-3G minimal basis set due to its computational cost [45,46]. Multiple lubricant chains of each Ztetraol and ZTMD were created using TopoTools in VMD [47] by matching the thicknesses of both lubricants at 14 Å to compare the effects of contaminants with different ratios of hydroxyl (–OH) endgroups. The multiple lubricant chains were then equilibrated in a canonical ensemble (NVT) at 300 K for 100 picoseconds after placing them on the 100 Å × 100 Å × 20 Å amorphous carbon substrate.

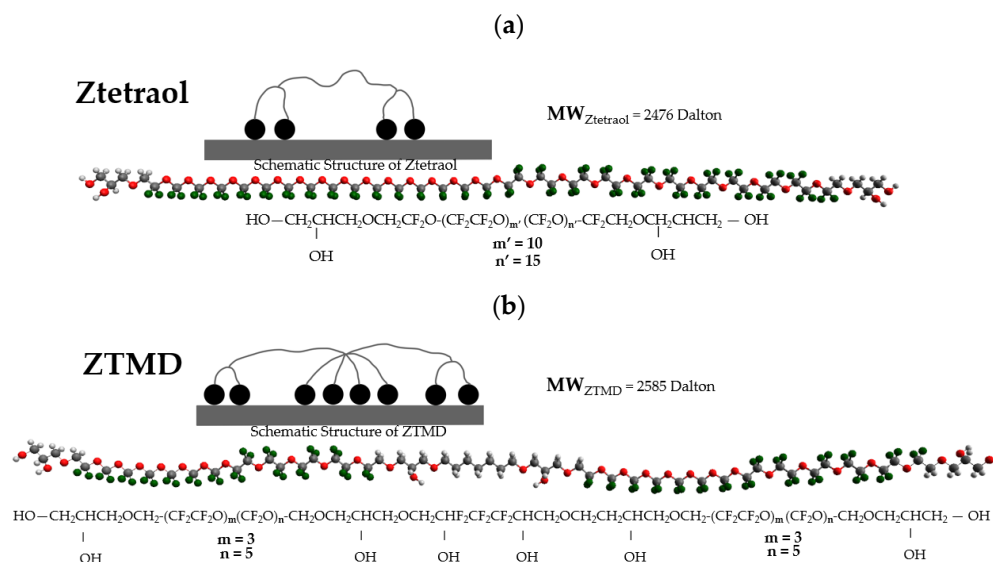


**Figure 1.** Schematic structure of a lubricant chain on the DLC surface, molecular weight, and chemical structure of (a) Ztetraol and (b) ZTMD. In the schematic, the black sphere and the line in between represent the –OH endgroup and backbone of a PFPE lubricant, respectively.

### 2.2.2. Substrate and Head Preparation

An amorphous carbon (i.e., diamond-like-carbon (DLC)) film was prepared with dimensions of 100 Å (W) × 100 Å (L) × 20 Å (H), on which PFPE lubricants were deposited. A cylindrical DLC tip with a hemispherical end was prepared with a 5 Å radius and 50 Å length, which was used for the sliding contact simulation. These two DLC materials were prepared using the liquid quenching method with a density of 2.2 g/cm<sup>3</sup> [48].

### 2.2.3. Contaminant Deposition

To avoid the escape of contaminant molecules out of the simulation box, the prepared chemical contaminants were placed in between the top bare DLC film and the bottom lubricated DLC film with a gap distance of 65 Å. An indirect heat bath method was chosen and applied on both DLC films, i.e., heating a microcanonical ensemble (NVE) with a canonical ensemble (NVT) as a heat bath, as shown in Figure 2, because direct heating in a system can increase the potential energy infinitely [49]. To adsorb the contaminants onto the PFPE lubricants, a randomly distributed set of SiO<sub>2</sub> and H<sub>2</sub>O molecules (1 set = 256 molecules) was placed in the gap, and then the equilibration proceeded at 300 K and 700 K for 200 ps. To achieve the relevant amount of SiO<sub>2</sub> contamination, four sets of SiO<sub>2</sub> contaminants were applied in sequence, while two sets of H<sub>2</sub>O contaminants were applied. In order to accelerate the reaction between the lubricant and water molecules, supersaturation conditions were chosen for each set of H<sub>2</sub>O contaminants in the gap, having supersaturation ratios of 500 and 125 at 300 K and 700 K, respectively, where the supersaturation ratio is the density of the applied water vapor over the density of saturated water vapor [50–52].

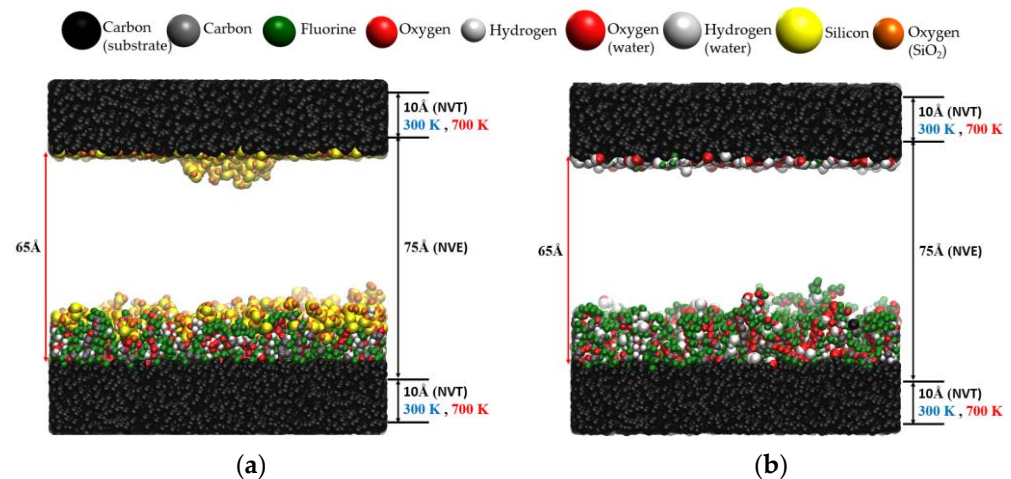


**Figure 2.** (a) SiO<sub>2</sub> and (b) H<sub>2</sub>O contaminants were adsorbed on to the PFPE lubricant at 300 K and 700 K.

### 2.3. Airshear Simulation

In order to evaluate and quantify the change in the mechano-chemical properties of the PFPE lubricants by the adsorbed contaminants, an airshear simulation was performed. Due to the high circumferential speed of hard disk drives (HDDs), there were strong air flows over the lubricants at the HDI in both the normal and tangential directions [53]. As shown in Figure 3, for the contaminated and non-contaminated PFPE lubricants, a normal stress of 60 MPa and tangential stress of 300 MPa was applied to one-third of the top layer of the lubricant film. The applied stress was set to be higher than the actual stress value to better compare the resulting airshear behaviors, following a previous study [21].

### 2.4. Sliding Contact Simulation and Surface Contamination

In order to analyze the effects of contaminants on the tribological performance of the PFPE lubricants, a sliding contact simulation was carried out. As shown in Figure 4, the cylindrical DLC tip described in Section 2.2.2 was slowly approached until it reached half the thickness of the lubricant layer and then proceeded with the equilibration for 15 ps. Then, the DLC tip slid in a tangential direction at a speed of 0.8 Å/ps (=80 m/s) for 50 ps. After the sliding distance of 40 Å, the DLC tip was fully retracted. The surface contamination or lubricant pick-up was quantified by counting the number of molecules that were transferred to the DLC tip.

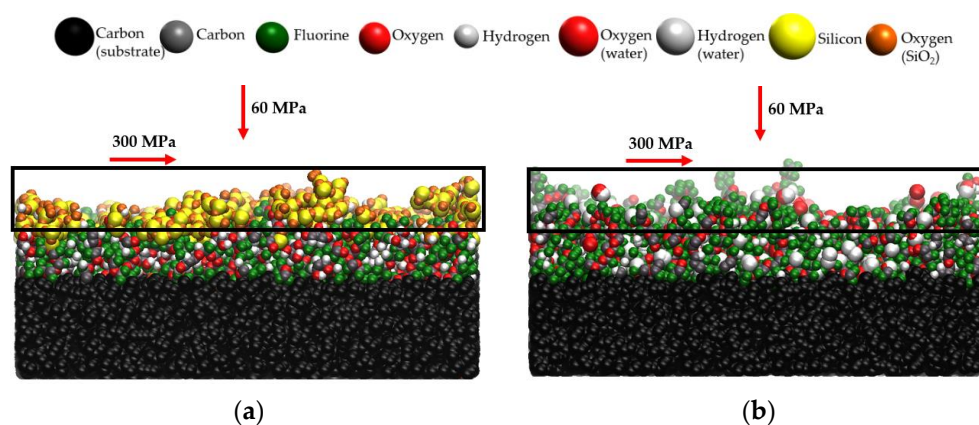


**Figure 3.** Schemes of the airshear simulation for (a) SiO<sub>2</sub>- and (b) H<sub>2</sub>O-contaminated PFPE lubricants.

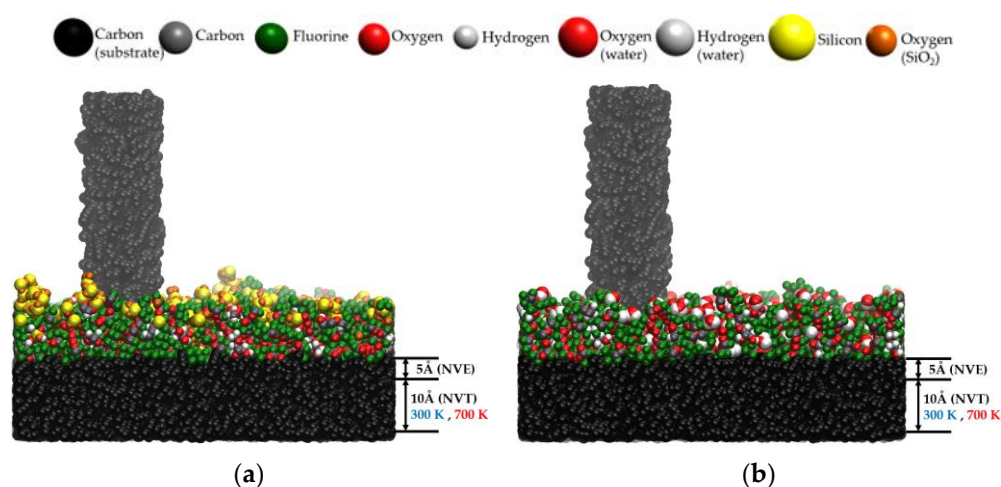


**Figure 4.** Schemes of the sliding contact simulation. A cylindrical DLC tip slides over the Ztetraol lubricants contaminated by (a) SiO<sub>2</sub> and (b) H<sub>2</sub>O.

### 3. Results and Discussion

#### 3.1. Adsorption of Silicon Dioxide (SiO<sub>2</sub>) and Water (H<sub>2</sub>O) Contaminants

As shown in Figure 3, after removing the top substrate, the adsorption of both silicon dioxide (SiO<sub>2</sub>) and water (H<sub>2</sub>O) contaminants was observed and quantified.

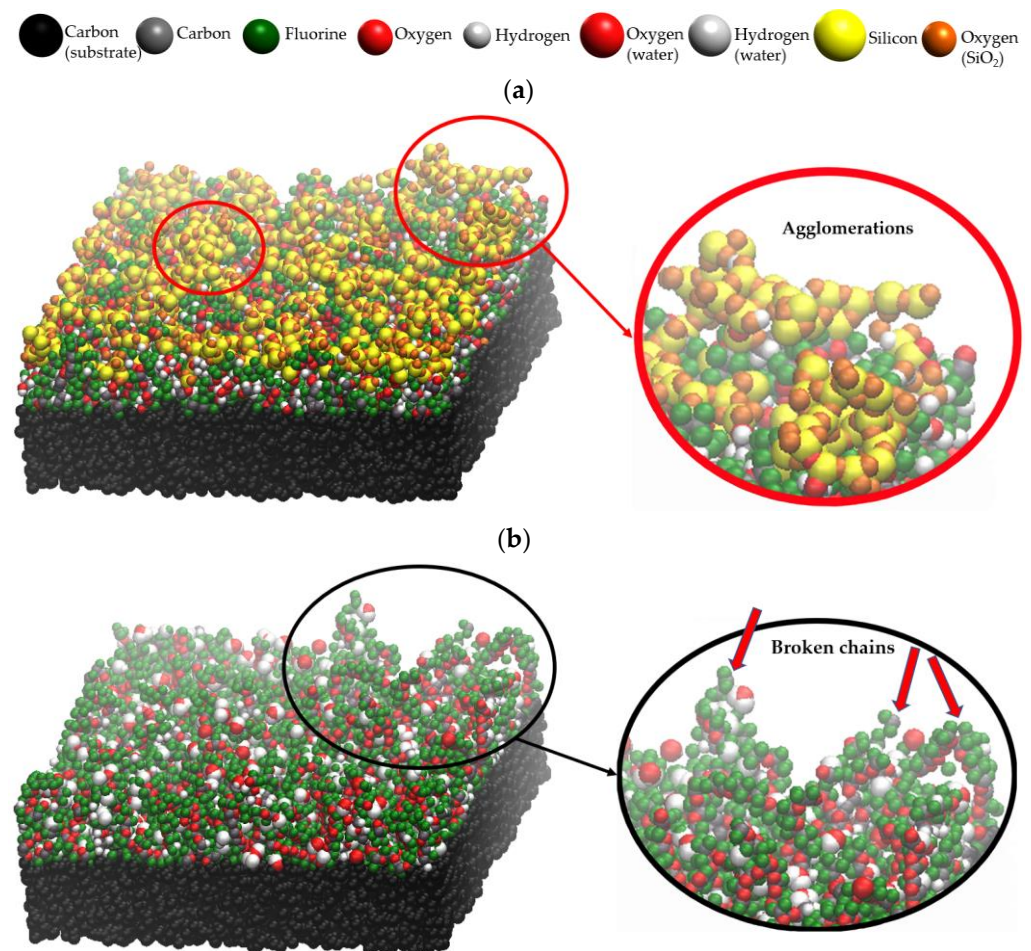
For both Ztetraol and ZTMD lubricants, the percentages of adsorbed SiO<sub>2</sub> contaminants were similar in 300 K and 700 K. However, for the case of H<sub>2</sub>O contaminants, the adsorption rate onto Ztetraol was higher than that of ZTMD by 13.8% at 300 K and 18.6% at 700 K, as summarized in Table 1. Also, when SiO<sub>2</sub> nanoparticles were adsorbed onto the PFPE lubricants, they did not physically damage the lubricant chains and showed agglomerative behaviors, as shown in Figure 5a, consistent with the previous study [21]. However, for H<sub>2</sub>O contamination, the adsorbed H<sub>2</sub>O molecules influenced the lubricant chains, causing critical bond breaks, as shown in Figure 5b.

The results in Table 1 provide a clue about the molecular interaction mechanisms of the SiO<sub>2</sub> and H<sub>2</sub>O contaminants within PFPE lubricants. SiO<sub>2</sub> contaminants tend to agglomerate with a higher bonding preference themselves, which potentially affects the mechanical behavior and lubricity of PFPE lubricants due to their large molecular property. On the contrary, H<sub>2</sub>O contaminants undergo significant reactions with Ztetraol. In addition, it was observed that the adsorption rates of SiO<sub>2</sub> and H<sub>2</sub>O contaminants slightly decreased at the higher temperature of 700 K. This can be explained by the fact that the affinities of contaminants and the adsorption capacity tend to decrease at higher temperatures, because the higher thermal energy increases the kinetic energy in the system.

**Table 1.** Adsorption rates of SiO<sub>2</sub> and H<sub>2</sub>O contaminants on Ztetraol and ZTMD at 300 K and 700 K.

Lubricants + Contaminants	Percentage of Atoms Adsorbed (%)
Ztetraol + SiO <sub>2</sub> at 300 K	67.1%
Ztetraol + SiO <sub>2</sub> at 700 K	64.9%
ZTMD + SiO <sub>2</sub> at 300 K	66.3%
ZTMD + SiO <sub>2</sub> at 700 K	64.4%
Ztetraol + H <sub>2</sub> O at 300 K	66.2%
Ztetraol + H <sub>2</sub> O at 700 K	63.9%
ZTMD + H <sub>2</sub> O at 300 K	58.2%
ZTMD + H <sub>2</sub> O at 700 K	53.9%

In the table, the percentages of atoms adsorbed were obtained by the number of contaminant atoms adsorbed over the total number of the applied contaminant atoms for SiO<sub>2</sub> (3072 atoms) and H<sub>2</sub>O (1536 atoms).

**Figure 5.** (a) SiO<sub>2</sub> and (b) H<sub>2</sub>O contaminants deposited in Ztetraol at 300 K.

### 3.2. Quantification of Airshear Behavior

The normal and tangential stresses (i.e., 60 MPa and 300 MPa, respectively) were applied to the prepared lubricated film samples for 100 ps. As shown in Figure 6, the resulting shear displacement was obtained by comparing the positions of lubricant atoms before and after applying the stresses. Since the lubricant molecules have stronger bonds to the underlying DLC surface through polar interactions, the shear displacement is mostly observed on the top layer of the lubricant. It was found that the PFPE lubricants (Ztetraol and ZTMD in this study) became stiffened by SiO<sub>2</sub> nanoparticles, having a limited amount of airshear displacement (Figure 6a), while water molecules significantly degraded and weakened the PFPE lubricants, causing greater airshear movement (Figure 6b).

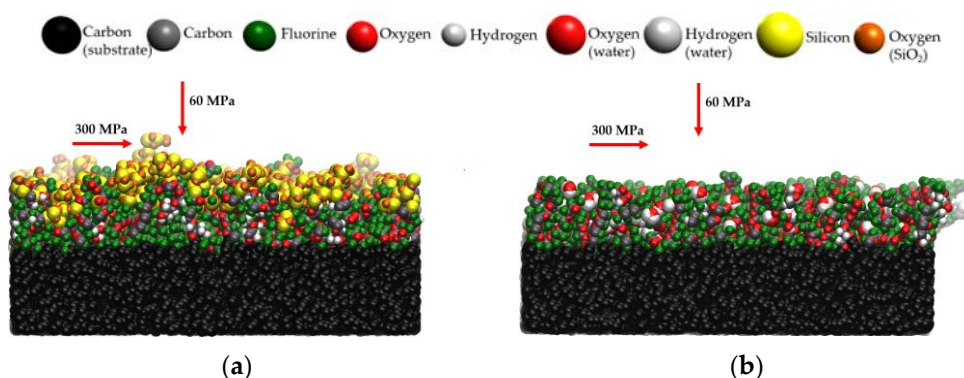


**Figure 6.** Visualizations of airshear behaviors for the Ztetraol lubricant at 300 K contaminated by (a) silicon dioxide (SiO<sub>2</sub>) and (b) water (H<sub>2</sub>O).

Figure 7 summarizes the resulting airshear displacement for the two PFPE lubricants (Ztetraol and ZTMD) contaminated by SiO<sub>2</sub> and H<sub>2</sub>O contaminants at 300 K, and the airshear behaviors for non-contaminated lubricants are included as a reference. Firstly, ZTMD showed much less airshear displacement than Ztetraol. This is attributed to its higher ratio of the hydroxyl endgroup in the molecular structure, enabling it to bond more strongly to the underlying DLC surface and the neighboring lubricant chains. Next, when SiO<sub>2</sub> nanoparticles were adsorbed onto the PFPE lubricants, they did not directly break or weaken the lubricant chains but were more likely to agglomerate with the lubricant layer. Accordingly, the lubricant layer became stiffened and more stress-resistant, leading to less airshear displacement. In Figure 7, for both Ztetraol and ZTMD, SiO<sub>2</sub> contaminants decreased the airshear displacement by 60.7% and 47.3%, respectively, compared to the result of non-contaminated lubricants. On the contrary, when H<sub>2</sub>O molecules were adsorbed onto the PFPE lubricants, they weakened and broke the interacting lubricant chains, making the whole lubricant layer more mobile. Compared to the non-contaminated lubricants, H<sub>2</sub>O contaminants increased the airshear displacement by 21.8% and 10.4% for Ztetraol and ZTMD, respectively. The following sections discuss the degradation mechanism of PFPE lubricants by H<sub>2</sub>O contamination.

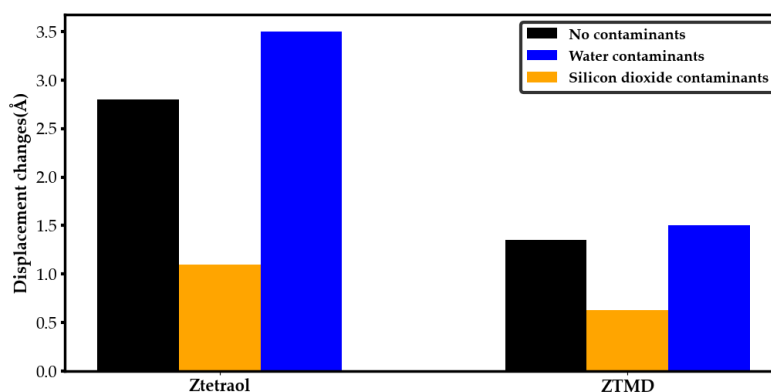


**Figure 7.** Airshear displacement changes on non-contaminated lubricants, SiO<sub>2</sub> and H<sub>2</sub>O contaminant deposited lubricants.

### 3.3. Analysis of Radial Distribution Functions (RDFs) and the Potential Energy Surface (PES)

In order to investigate the interactions among the PFPE lubricant and contaminants, radial distribution functions were obtained for the Ztetraol lubricant with and without contaminants (i.e., SiO<sub>2</sub> and H<sub>2</sub>O) through LAMMPS [38]. Figure 8 shows the RDF results for the possible covalent bonds, including C<sub>backbone</sub>-C<sub>backbone</sub>, C<sub>backbone</sub>-O<sub>backbone</sub>, C<sub>backbone</sub>-H<sub>backbone</sub>, C<sub>backbone</sub>-O<sub>endgroup</sub>, and O<sub>endgroup</sub>-H<sub>endgroup</sub>.

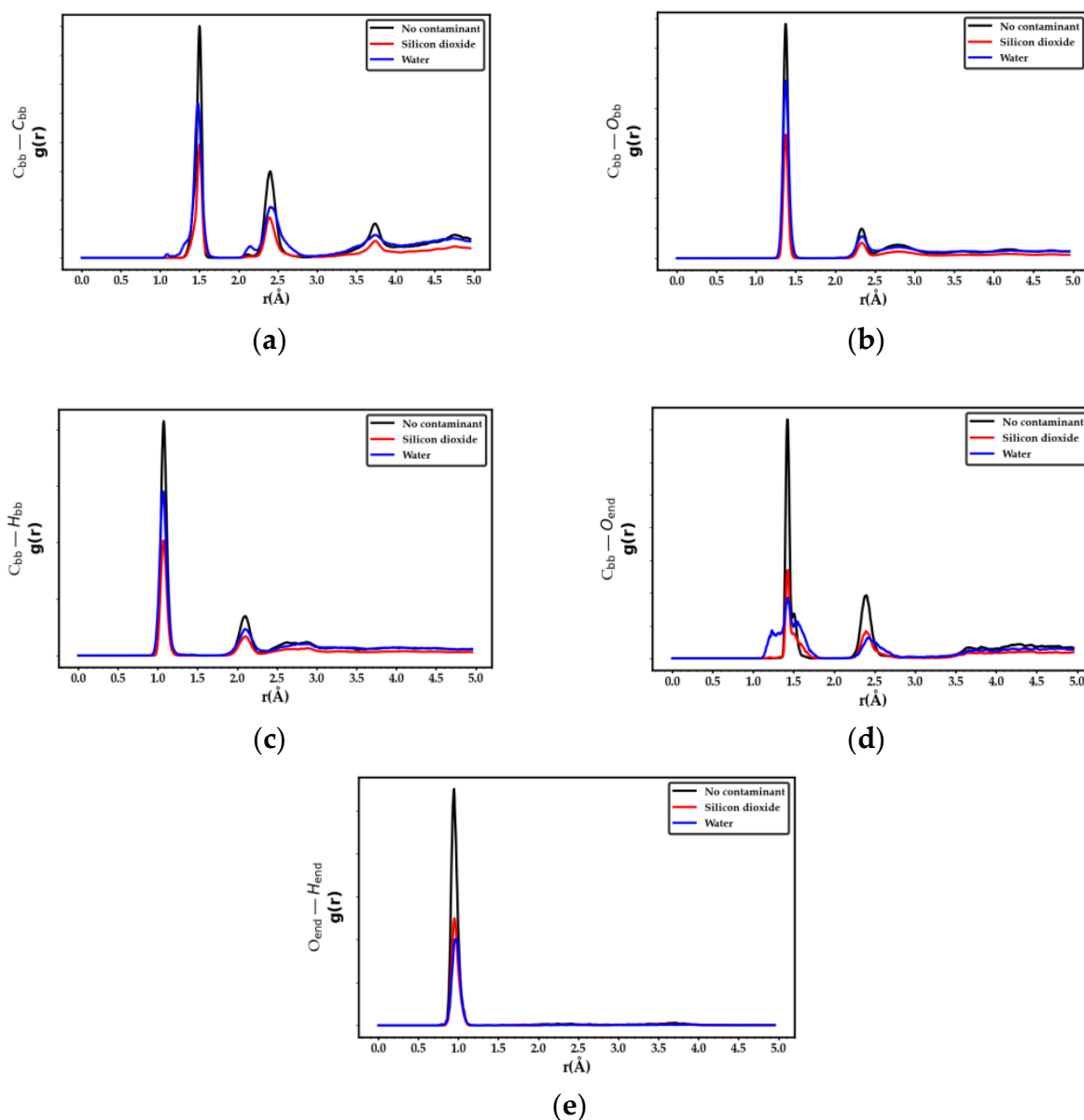


**Figure 8.** RDFs for the possible covalent bonds in the Ztetraol lubricant: (a) carbon (backbone)–carbon (backbone), (b) carbon (backbone)–oxygen (backbone), (c) carbon (backbone)–hydrogen (backbone), (d) carbon (backbone)–oxygen (endgroup), and (e) oxygen (endgroup)–hydrogen (endgroup).

It is noted that the radial distance corresponding to each peak represents the distance between a pair of atoms, while the amplitude of the peak is the probability of occurrence. For the backbone of Ztetraol (Figure 8a–c), it was observed that both contaminated and non-contaminated lubricants showed consistent peak positions, whereas the probability of occurrence was in the order of non-contaminant > H<sub>2</sub>O > SiO<sub>2</sub>. The consistent order and matching radius of each peak indicate limited reactions in the  $C_{backbone}-C_{backbone}$ ,  $C_{backbone}-O_{backbone}$ , and  $C_{backbone}-H_{backbone}$  bonds, but the larger molecule sizes of the SiO<sub>2</sub> and H<sub>2</sub>O contaminants decreased the probability of occurrence. The  $C_{backbone}-O_{endgroup}$  bond in Figure 8d has a bonding length of ~1.43 Å in its normal state. When H<sub>2</sub>O contaminants were adsorbed onto the Ztetraol, broader peak near 1.43 Å was produced. This implies that the adsorbed H<sub>2</sub>O molecules changed and weakened the  $C_{backbone}-O_{endgroup}$  bonds, thereby degrading the Ztetraol lubricant. Also, the RDF for the  $O_{endgroup}-H_{endgroup}$  bond showed different results from the bonds in the backbone. In Figure 8e, the probability of

occurrence for the  $O_{\text{endgroup}}-H_{\text{endgroup}}$  bond is the lowest under  $H_2O$  contaminants, which provides evidence of lubricant degradation by  $H_2O$  contaminants.

Next, to investigate the degrading mechanism of the PFPE lubricant by  $H_2O$  molecules, a potential energy surface (PES) was calculated using the automated PES exploration tool of AMS2022.101 software [54,55] and redrawn using Matplotlib in Python [56], as shown in Figure 9. The PES supports the idea of the degradation of the  $C_{\text{backbone}}-O_{\text{endgroup}}$  bond by showing possible reactions to how a  $H_2O$  molecule can influence degradation at the hydroxyl end group. According to the PES calculation, the following procedures describe the most probable degradation mechanism. Firstly, a water molecule attracts a hydrogen atom in the carbon, causing the  $C-H$  bond to break, and then the hydrogen atom bonds to the hydroxyl end group, forming a  $H_2O$  molecule, which breaks the  $C_{\text{backbone}}-O_{\text{endgroup}}$  bond break.

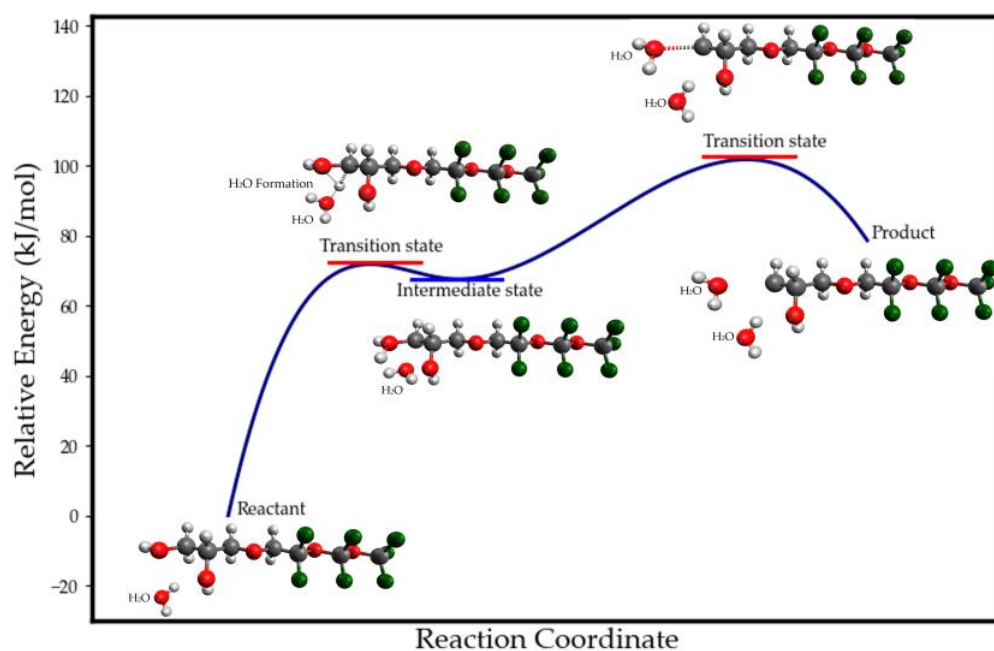


**Figure 9.** Potential energy surface (PES) curve for one of the hypothetical reactions between the  $H_2O$  contaminant and the hydroxyl endgroup( $-OH$ ) of the PFPE lubricants.

### 3.4. Quantification of Lubricant Degradation with Water ( $H_2O$ ) Contaminants

To confirm the RDF results presented in Section 3.3 and further investigate the degradation mechanism of PFPE lubricants by  $H_2O$  molecules, we analyzed the atomic interactions between  $H_2O$  molecules and two PFPE lubricants (i.e., Ztetraol and ZTMD) at 300 K using VMD simulations. A strand of Ztetraol consists of 16  $C_{\text{bb}}-C_{\text{bb}}$ , 74  $C_{\text{bb}}-F_{\text{bb}}$ , 14  $C_{\text{bb}}-H_{\text{bb}}$ , 56  $C_{\text{bb}}-O_{\text{bb}}$ , 4  $C_{\text{bb}}-O_{\text{end}}$ , and 4  $O_{\text{end}}-H_{\text{end}}$  bonds, while a strand of ZTMD includes 26  $C_{\text{bb}}-C_{\text{bb}}$ , 70  $C_{\text{bb}}-F_{\text{bb}}$ , 34  $C_{\text{bb}}-H_{\text{bb}}$ , 56  $C_{\text{bb}}-O_{\text{bb}}$ , 8  $C_{\text{bb}}-O_{\text{end}}$ , and 8  $O_{\text{end}}-H_{\text{end}}$  bonds. Table 2 summarizes the quantified degradation of lubricant bonds. This study quantified the degradation of Ztetraol and ZTMD under  $H_2O$ -contaminated conditions using VMD. Every strand of Ztetraol and ZTMD was checked to quantify degradation, with the interatomic distance of 5 Å considered to be a bond break influenced by  $H_2O$  molecules. It was observed that when  $H_2O$  molecules were adsorbed onto the Ztetraol lubricant, the two endgroup-related bonds, i.e.,  $O_{\text{endgroup}}-H_{\text{endgroup}}$  and  $C_{\text{backbone}}-O_{\text{endgroup}}$  bonds, dominantly contributed to the degradation of the lubricant. In Table 2(a), these two bonds became weakened and lost their ability to anchor onto the DLC substrate. Compared to the Ztetraol lubricant, ZTMD showed superior resistance to the adsorbed water molecules, as shown in Table 2(b). Considering that ZTMD lubricants have more  $-OH$  endgroups and a stronger bonding preference themselves, they might not be less reactive to the incoming  $H_2O$  molecules than Ztetraol.

**Table 2.** Quantification of PFPE lubricant degradation: (a) Ztetraol + H<sub>2</sub>O at 300 K and (b) ZTMD + H<sub>2</sub>O at 300 K.

(a) Ztetraol + H <sub>2</sub> O at 300K:						
	C <sub>bb</sub> -C <sub>bb</sub>	C <sub>bb</sub> -F <sub>bb</sub>	C <sub>bb</sub> -H <sub>bb</sub>	C <sub>bb</sub> -O <sub>bb</sub>	C <sub>bb</sub> -O <sub>end</sub>	O <sub>end</sub> -H <sub>end</sub>
No. of Degraded bonds	5	136	64	12	73	98
% of Degradation	3.06%	0.52%	7.62%	0.36%	30.42%	40.83%
(b) ZTMD + H <sub>2</sub> O at 300 K:						
	C <sub>bb</sub> -C <sub>bb</sub>	C <sub>bb</sub> -F <sub>bb</sub>	C <sub>bb</sub> -H <sub>bb</sub>	C <sub>bb</sub> -O <sub>bb</sub>	C <sub>bb</sub> -O <sub>end</sub>	O <sub>end</sub> -H <sub>end</sub>
No. of Degraded bonds	5	136	64	12	73	98
% of Degradation	3.06%	0.52%	7.62%	0.36%	30.42%	40.83%

In the table, the percentages of degradation were obtained by the number of bond breakages over the total number of bonds. Ztetraol: 960C<sub>bb</sub>-C<sub>bb</sub>, 4440C<sub>bb</sub>-F<sub>bb</sub>, 840C<sub>bb</sub>-H<sub>bb</sub>, 3360C<sub>bb</sub>-O<sub>bb</sub>, 240C<sub>bb</sub>-O<sub>end</sub>, and 240O<sub>end</sub>-H<sub>end</sub> bonds and ZTMD: 1300C<sub>bb</sub>-C<sub>bb</sub>, 3500C<sub>bb</sub>-F<sub>bb</sub>, 1700C<sub>bb</sub>-H<sub>bb</sub>, 2800C<sub>bb</sub>-O<sub>bb</sub>, 400C<sub>bb</sub>-O<sub>end</sub>, and 400O<sub>end</sub>-H<sub>end</sub> bonds.

### 3.5. Friction Force Measurement during Sliding Contact

As explained in Section 2.4 and Figure 4, a cylindrical nano-DLC tip slid over the PFPE lubricants at a speed of 0.8 Å/ps (=80 m/s), and the resulting friction force was measured. Figure 10 shows the resulting friction force measured at 300 K and 700 K. Compared to the friction force for the non-contaminated lubricant, SiO<sub>2</sub> contaminants significantly increased the friction force of the Ztetraol and ZTMD lubricants by 149% and 89%, respectively, at 300 K and 282% and 120%, respectively, at 700 K. This is consistent with the airshear simulation results presented in Section 3.2, because SiO<sub>2</sub> nanoparticles stiffened the PFPE lubricants, causing higher friction force during sliding contact. On the contrary, H<sub>2</sub>O contaminants decreased the friction force of Ztetraol by 17.9% and 21.1% at 300 K and 700 K, respectively. Even though the H<sub>2</sub>O-contaminated Ztetraol produced lower friction than the non-contaminated Ztetraol, this also implies that it can have a better chance of making direct solid-to-solid contacts if the contact load is high enough for the tip to penetrate the lubricant layer. In the case of the ZTMD lubricant, since it does not have critical reactions with H<sub>2</sub>O contaminants, its friction force was not much different from the value of the non-contaminated ZTMD lubricant.

### 3.6. Surface Contamination by Lubricant Pick-Up

Another issue to consider for a surface-protecting lubricant is the contamination of the counteracting surface during sliding contact. As shown in Figure 11, the cylindrical DLC tip was fully retracted from the contacting surface after completing the sliding contact. Then, the amount of picked-up lubricant was quantitatively measured. Firstly, as shown in Figure 12, SiO<sub>2</sub> contaminants increased the number of lubricant pick-ups for both Ztetraol and ZTMD lubricants. As discussed in a previous study [16], SiO<sub>2</sub> contaminants have a strong bonding preference for the sliding DLC tip as well as the neighboring lubricant atoms. During the sliding contact, SiO<sub>2</sub> particles near the path of the DLC tip were bonded to the tip surface, which subsequently attracted the interacting neighboring lubricant molecules together, thereby increasing the number of transferred atoms to the DLC tip surface. Next, when H<sub>2</sub>O molecules were adsorbed onto Ztetraol, the number of lubricant pick-ups decreased. As described in Sections 3.3 and 3.4, H<sub>2</sub>O molecules tend to degrade and break the Ztetraol bonds. Accordingly, the broken pieces of lubricant were transferred to the DLC tip surface during the sliding contact, leading to fewer lubricant pick-ups. For

the case of ZTMD, as it does not react much with H<sub>2</sub>O contaminants, its lubricant pick-up behavior was similar to the non-contaminated condition.

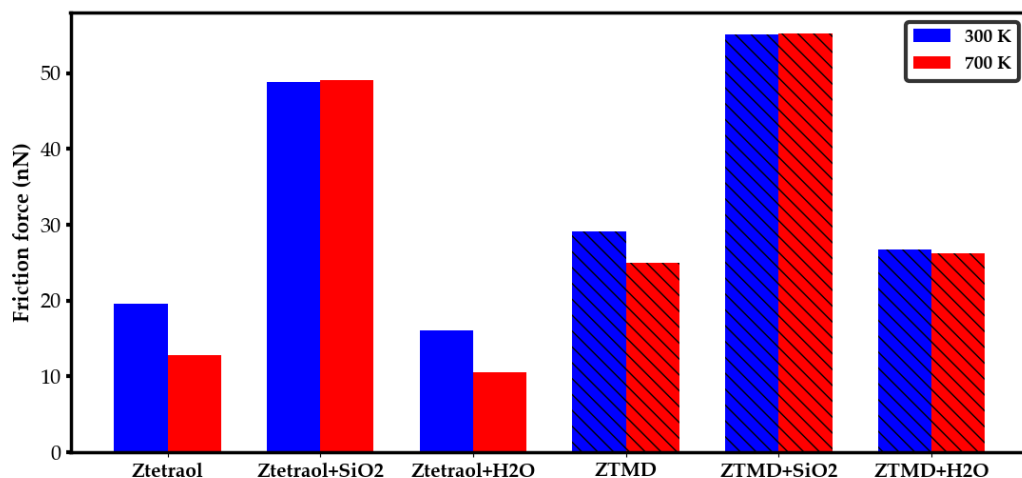


**Figure 10.** The measured friction force for the two PFPE lubricants with and without the SiO<sub>2</sub> and H<sub>2</sub>O contaminants at 300 K and 700 K. Note: Regular bars for Ztetraol and slanted bars are ZTMD lubricant.

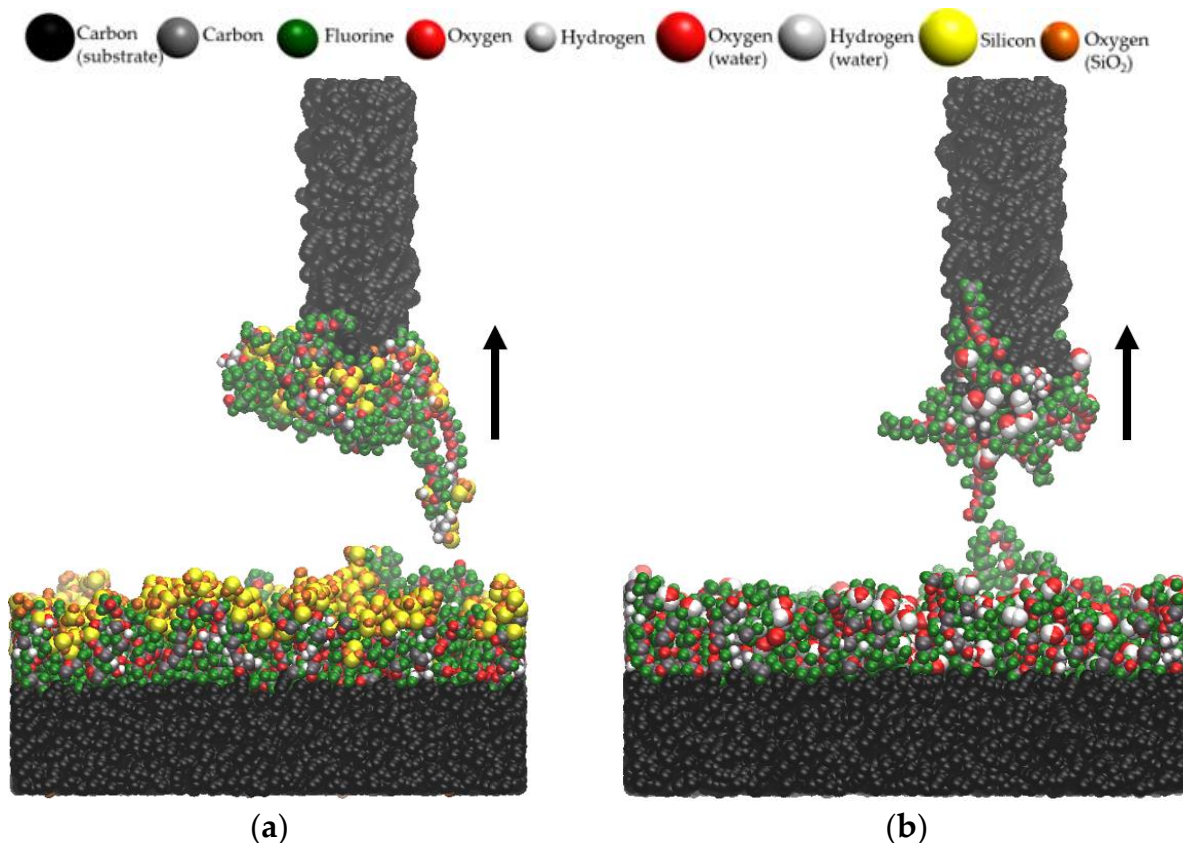


**Figure 11.** Simulation of the lubricant pick-up after the sliding contact through retraction in the direction of arrows for the Ztetraol lubricant contaminated by (a) SiO<sub>2</sub> and (b) H<sub>2</sub>O contaminants.

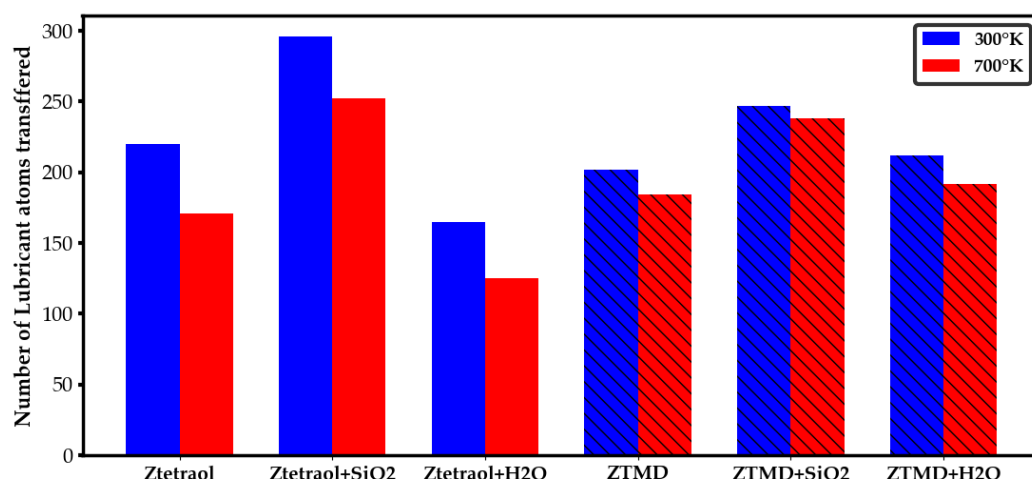


**Figure 12.** Quantification of lubricant atoms transferred after the retraction of the cylindrical head. Note: Regular bars for Ztetraol and slanted bars are ZTMD lubricant.

#### 4. Conclusions

This study investigated the mechano-chemical properties and tribological performance of Ztetraol and ZTMD lubricants under exposure to SiO<sub>2</sub> and H<sub>2</sub>O contaminants. When the two PFPE lubricants were exposed to SiO<sub>2</sub> contaminants, SiO<sub>2</sub> nanoparticles tended to agglomerate within the lubricant layer making the whole lubricant layer stiffer. Even though SiO<sub>2</sub> contaminants underwent strong bonding to the PFPE lubricants, they did not significantly degrade or break the lubricant chains. For this reason, there was higher friction but more lubricant pick-ups during sliding contact. Contrary to the SiO<sub>2</sub> contaminants, H<sub>2</sub>O molecules significantly changed the mechano-chemical properties of the Ztetraol lubricant. When H<sub>2</sub>O contaminants were adsorbed onto Ztetraol, the bonds in the hydroxyl endgroups, i.e., the C<sub>backbone</sub>–O<sub>endgroup</sub> and O<sub>endgroup</sub>–H<sub>endgroup</sub> bonds, were significantly degraded and broken. Accordingly, this degradation process led to larger airshear displacement, lower friction, and less lubricant pick-up behaviors. However, compared to Ztetraol, ZTMD showed limited reactions with H<sub>2</sub>O molecules, having more resistance to degradation. Therefore, from the outcome of this study, it can be found that the structural design of hydroxyl endgroups in PFPE lubricant is critical to protect its lubricity from external contaminants.

**Author Contributions:** Conceptualization, C.Y. and Y.J.; methodology, C.Y. and Y.J.; MD simulations; formal analysis and investigation, C.Y. and Y.J.; all authors contributed to the original draft preparation; project administration, C.Y. All authors have read and agreed to the published version of the manuscript.

**Funding:** This research was supported by Seagate Technology [Agreement Number 73592.0]. The authors gratefully acknowledge this support.

**Institutional Review Board Statement:** Not applicable.

**Informed Consent Statement:** Not applicable.

**Data Availability Statement:** Computational simulation code from this study is available from Changdong Yeo (email: changdong.yeo@ttu.edu) upon reasonable request.

**Conflicts of Interest:** The authors declare no conflict of interest.

#### References

- Zhang, W.; Friedman, B.A.; Bain, J.A. Simulation of a Thermally Efficient HAMR Ridge Waveguide NFT on an AIN Heat Sink. In Proceedings of the 2021 IEEE 32nd Magnetic Recording Conference (TMRC), Virtual, 16–19 August 2021; pp. 1–2.
- Rai, R.; Bhargava, P.; Knigge, B.; Murthy, A.N. A method for monitoring head media spacing change in a hard disk drive using an embedded contact sensor. *Microsyst. Technol.* **2020**, *26*, 3459–3467. [[CrossRef](#)]

3. Kiely, J.D.; Jones, P.M.; Yang, Y.; Brand, J.L.; Anaya-Dufresne, M.; Fletcher, P.C.; Zavaliche, F.; Toivola, Y.; Duda, J.C.; Johnson, M.T. Write-Induced Head Contamination in Heat-Assisted Magnetic Recording. *IEEE Trans. Magn.* **2017**, *53*, 1–7. [[CrossRef](#)]
4. Seo, Y.W.; Ovcharenko, A.; Bilich, D.; Talke, F.E. Experimental Investigation of Hydrocarbon Contamination at the Head-Disk Interface. *Tribol. Lett.* **2017**, *65*, 54. [[CrossRef](#)]
5. Kasai, P.H.; Eng, F.P. Silicon oxide formation in the disk environment. *J. Inf. Stor. Proc. Syst.* **2000**, *2*, 125–128.
6. Peng, D.X.; Chen, C.H.; Kang, Y.; Chang, Y.P.; Chang, S.Y. Size effects of SiO<sub>2</sub> nanoparticles as oil additives on tribology of lubricant. *Ind. Lubr. Tribol.* **2010**, *62*, 111–120. [[CrossRef](#)]
7. Qi, H.; Guo, Y.; Zhang, L.; Li, G.; Zhang, G.; Wang, T.; Wang, Q. Covalently attached mesoporous silica-ionic liquid hybrid nanomaterial as water lubrication additives for polymer-metal tribopair. *Tribol. Int.* **2018**, *119*, 721–730. [[CrossRef](#)]
8. Wang, N.; Wang, H.; Ren, J.; Gao, G.; Chen, S.; Zhao, G.; Yang, Y.; Wang, J. Novel additive of PTFE@SiO<sub>2</sub> core-shell nanoparticles with superior water lubricating properties. *Mater. Des.* **2020**, *195*, 109069. [[CrossRef](#)]
9. Wang, N.; Wang, H.; Ren, J.; Gao, G.; Zhao, G.; Yang, Y.; Wang, J. High-efficient and environmental-friendly PTFE@SiO<sub>2</sub> core-shell additive with excellent AW/EP properties in PAO6. *Tribol. Int.* **2021**, *158*, 106930. [[CrossRef](#)]
10. Liu, Y.; He, H.; Yang, M.; Zhang, R.; Yu, S.; Yang, T.; Wang, W.; Liang, F. Novel concept of nano-additive design: PTFE@silica Janus nanoparticles for water lubrication. *Friction* **2023**. [[CrossRef](#)]
11. Liu, N.; Bogy, D.B. Particle Contamination on a Thermal Flying-Height Control Slider. *Tribol. Lett.* **2009**, *37*, 93–97. [[CrossRef](#)]
12. Guo, X.C.; Raman, V.; Karis, T.E.; Yao, Y.Z. Flyability failures due to siloxanes at the head-disk interface revisited. *IEEE Trans. Magn.* **2007**, *43*, 2223–2225. [[CrossRef](#)]
13. Liu, Q.K.; Li, L.Q.; Zhang, G.Y.; Shuai, C.J. Study on Failure Process of Silicon-Doped Amorphous Carbon by ReaxFF Molecular Dynamics Simulation for HAMR. *Ieee Trans. Magn.* **2020**, *56*, 7502706. [[CrossRef](#)]
14. Zhao, Z.; Bhushan, B. Effect of environmental humidity on the friction/stiction and durability of lubricated magnetic thin-film disks. *Part I Mech. Eng. J.-J. Eng.* **1997**, *211*, 295–301. [[CrossRef](#)]
15. Zhao, Z.M.; Bhushan, B. Tribological performance of PFPE and X-1P lubricants at head-disk interface. Part I. Experimental results. *Tribol. Lett.* **1999**, *6*, 129–139. [[CrossRef](#)]
16. Zhao, Z.M.; Bhushan, B.; Kajdas, C. Tribological performance of PFPE and X-1P lubricants at head-disk interface. Part II. Mechanisms. *Tribol. Lett.* **1999**, *6*, 141–148. [[CrossRef](#)]
17. Tyndall, G.W.; Waltman, R.J.; Pacansky, J. Effect of adsorbed water on perfluoropolyether-lubricated magnetic recording disks. *J. Appl. Phys.* **2001**, *90*, 6287–6296. [[CrossRef](#)]
18. Karis, T.E. Water adsorption on thin film media. *J. Colloid. Interf. Sci.* **2000**, *225*, 196–203. [[CrossRef](#)]
19. Dai, Q.; Vurens, G.; Luna, M.; Salmeron, M. Lubricant distribution on hard disk surfaces: Effect of humidity and terminal group reactivity. *Langmuir* **1997**, *13*, 4401–4406. [[CrossRef](#)]
20. Liu, H.W.; Bhushan, B. Nanotribological characterization of molecularly thick lubricant films for applications to MEMS/NEMS by AFM. *Ultramicroscopy* **2003**, *97*, 321–340. [[CrossRef](#)]
21. Rahman, S.; Purani, D.; Ali, S.; Yeo, C.D. Effects of SiO<sub>2</sub> Contaminant on Thermo-Mechanical/Chemical Properties and Lubricity of PFPE Lubricants. *Lubricants* **2021**, *9*, 90. [[CrossRef](#)]
22. Li, L.; Jones, P.M.; Hsia, Y.T. Effect of chemical structure and molecular weight on high-temperature stability of some Fomblin Z-type lubricants. *Tribol. Lett.* **2004**, *16*, 21–27. [[CrossRef](#)]
23. Bhushan, B. Magnetic Media Tribology—State-of-the-Art and Future Challenges. *Wear* **1990**, *136*, 169–197. [[CrossRef](#)]
24. O’Hagan, D. Understanding organofluorine chemistry. An introduction to the C-F bond. *Chem. Soc. Rev.* **2008**, *37*, 308–319. [[CrossRef](#)]
25. Erdemir, A.; Ramirez, G.; Eryilmaz, O.L.; Narayanan, B.; Liao, Y.F.; Kamath, G.; Sankaranarayanan, S.K.R.S. Carbon-based tribofilms from lubricating oils. *Nature* **2016**, *536*, 67–71. [[CrossRef](#)]
26. Guo, X.C.; Knigge, B.; Marchon, B.; Waltman, R.J.; Carter, M.; Burns, J. Multidentate functionalized lubricant for ultralow head/disk spacing in a disk drive. *J. Appl. Phys.* **2006**, *100*, 044306. [[CrossRef](#)]
27. Ghahri Sarabi, M.S.; Bogy, D.B. Simulation of the Performance of Various PFPE Lubricants Under Heat Assisted Magnetic Recording Conditions. *Tribol. Lett.* **2014**, *56*, 293–304. [[CrossRef](#)]
28. Xiong, S.; Bogy, D.B. Experimental Study of Head-Disk Interface in Heat-Assisted Magnetic Recording. *IEEE Trans. Magn.* **2014**, *50*, 148–154. [[CrossRef](#)]
29. Sakhalkar, S.V.; Bogy, D.B. A Model for Lubricant Transfer from Media to Head during Heat-Assisted Magnetic Recording (HAMR) Writing. *Tribol. Lett.* **2017**, *65*, 166. [[CrossRef](#)]
30. Chen, X.; Kawai, K.; Zhang, H.; Fukuzawa, K.; Koga, N.; Itoh, S.; Azuma, N. ReaxFF Reactive Molecular Dynamics Simulations of Mechano-Chemical Decomposition of Perfluoropolyether Lubricants in Heat-Assisted Magnetic Recording. *J. Phys. Chem. C* **2020**, *124*, 22496–22505. [[CrossRef](#)]
31. van Duin, A.C.T.; Dasgupta, S.; Lorant, F.; Goddard, W.A. ReaxFF: A reactive force field for hydrocarbons. *J. Phys. Chem. A* **2001**, *105*, 9396–9409. [[CrossRef](#)]
32. Chenoweth, K.; van Duin, A.C.T.; Goddard, W.A. ReaxFF reactive force field for molecular dynamics simulations of hydrocarbon oxidation. *J. Phys. Chem. A* **2008**, *112*, 1040–1053. [[CrossRef](#)] [[PubMed](#)]
33. Ashraf, C.; van Duin, A.C.T. Extension of the ReaxFF Combustion Force Field toward Syngas Combustion and Initial Oxidation Kinetics. *J. Phys. Chem. A* **2017**, *121*, 1051–1068. [[CrossRef](#)] [[PubMed](#)]

34. Cheng, T.; Jaramillo-Botero, A.; Goddard, W.A.; Sun, H. Adaptive Accelerated ReaxFF Reactive Dynamics with Validation from Simulating Hydrogen Combustion. *J. Am. Chem. Soc.* **2014**, *136*, 13467. [CrossRef]
35. Chipara, A.C.; Tsafack, T.; Owuor, P.S.; Yeon, J.; Junkermeier, C.E.; van Duin, A.C.T.; Bhowmick, S.; Asif, S.A.S.; Radhakrishnan, S.; Park, J.H.; et al. Underwater adhesive using solid-liquid polymer mixes. *Mater. Today Chem.* **2018**, *9*, 149–157. [CrossRef]
36. Srinivasan, S.G.; van Duin, A.C.T. Molecular-Dynamics-Based Study of the Collisions of Hyperthermal Atomic Oxygen with Graphene Using the ReaxFF Reactive Force Field. *J. Phys. Chem. A* **2011**, *115*, 13269–13280. [CrossRef]
37. Chenoweth, K.; Cheung, S.; van Duin, A.C.T.; Goddard, W.A.; Kober, E.M. Simulations on the thermal decomposition of a poly(dimethylsiloxane) polymer using the ReaxFF reactive force field. *J. Am. Chem. Soc.* **2005**, *127*, 7192–7202. [CrossRef]
38. Thompson, A.P.; Aktulga, H.M.; Berger, R.; Bolintineanu, D.S.; Brown, W.M.; Crozier, P.S.; Veld, P.J.I.; Kohlmeyer, A.; Moore, S.G.; Nguyen, T.D.; et al. LAMMPS—a flexible simulation tool for particle-based materials modeling at the atomic, meso, and continuum scales. *Comput. Phys. Commun.* **2022**, *271*, 108171. [CrossRef]
39. Hanwell, M.D.; Curtis, D.E.; Lonie, D.C.; Vandermeersch, T.; Zurek, E.; Hutchison, G.R. Avogadro: An advanced semantic chemical editor, visualization, and analysis platform. *J. Cheminform* **2012**, *4*, 17. [CrossRef]
40. Chung, P.; Vemuri, S.; Jhon, M.S. Atomistic and Molecular Effects on the Surface Morphology and Film Conformation of Perfluoropolyether Lubricant Layer. *IEEE Trans. Magn.* **2015**, *51*, 3300904. [CrossRef]
41. Song, J.A.; Talukder, S.; Rahman, S.M.; Jung, Y.N.; Yeo, C.D. Comparison study on surface and thermo-chemical properties of PFPE lubricants on DLC film through MD simulations. *Tribol. Int.* **2021**, *156*, 106835. [CrossRef]
42. Apra, E.; Bylaska, E.J.; de Jong, W.A.; Govind, N.; Kowalski, K.; Straatsma, T.P.; Valiev, M.; van Dam, H.J.J.; Alexeev, Y.; Anchell, J.; et al. NWChem: Past, present, and future. *J. Chem. Phys.* **2020**, *152*, 184102. [CrossRef] [PubMed]
43. Becke, A.D. Density-functional exchange-energy approximation with correct asymptotic behavior. *Phys. Rev. A Gen. Phys.* **1988**, *38*, 3098–3100. [CrossRef]
44. Mulliken, R.S. Electronic Population Analysis on Lcao-Mo Molecular Wave Functions.1. *J. Chem. Phys.* **1955**, *23*, 1833–1840. [CrossRef]
45. Hehre, W.J.; Stewart, R.F.; Pople, J.A. Self-Consistent Molecular-Orbital Methods.I. Use of Gaussian Expansions of Slater-Type Atomic Orbitals. *J. Chem. Phys.* **1969**, *51*, 2657–2664. [CrossRef]
46. Collins, J.B.; Schleyer, P.V.; Binkley, J.S.; Pople, J.A. Self-Consistent Molecular-Orbital Methods.17. Geometries and Binding-Energies of 2nd-Row Molecules—Comparison of 3 Basis Sets. *J. Chem. Phys.* **1976**, *64*, 5142–5151. [CrossRef]
47. Humphrey, W.; Dalke, A.; Schulten, K. VMD: Visual molecular dynamics. *J. Mol. Graph. Model.* **1996**, *14*, 33–38. [CrossRef] [PubMed]
48. Galli, G.; Martin, R.M.; Car, R.; Parrinello, M. Structural and Electronic-Properties of Amorphous-Carbon. *Phys. Rev. Lett.* **1989**, *62*, 555–558. [CrossRef]
49. Janke, W.; Schierz, P.; Zierenberg, J. Transition barrier at a first-order phase transition in the canonical and microcanonical ensemble. *J. Phys. Conf. Ser.* **2017**, *921*, 012018. [CrossRef]
50. Bauer, B.A.; Patel, S. Properties of water along the liquid-vapor coexistence curve via molecular dynamics simulations using the polarizable TIP4P-QDP-LJ water model. *J. Chem. Phys.* **2009**, *131*, 084709. [CrossRef]
51. Branco, R.J.; Graber, M.; Denis, V.; Pleiss, J. Molecular mechanism of the hydration of Candida antarctica lipase B in the gas phase: Water adsorption isotherms and molecular dynamics simulations. *Chembiochem* **2009**, *10*, 2913–2919. [CrossRef]
52. Jain, S.; Qiao, L. Molecular dynamics simulations of the surface tension of oxygen-supersaturated water. *AIP Adv.* **2017**, *7*, 045001. [CrossRef]
53. Wu, L. Modeling and simulation of the interaction between lubricant droplets on the slider surface and air flow within the head/disk interface of disk drives. *IEEE Trans. Magn.* **2006**, *42*, 2480–2482. [CrossRef]
54. SCM. AMS 2022.101. Available online: <http://www.scm.com> (accessed on 18 April 2022).
55. Chill, S.T.; Welborn, M.; Terrell, R.; Zhang, L.; Berthet, J.C.; Pedersen, A.; Jonsson, H.; Henkelman, G. EON: Software for long time simulations of atomic scale systems. *Model. Simul. Mater. Sc.* **2014**, *22*, 055002. [CrossRef]
56. Hunter, J.D. Matplotlib: A 2D graphics environment. *Comput. Sci. Eng.* **2007**, *9*, 90–95. [CrossRef]

**Disclaimer/Publisher’s Note:** The statements, opinions and data contained in all publications are solely those of the individual author(s) and contributor(s) and not of MDPI and/or the editor(s). MDPI and/or the editor(s) disclaim responsibility for any injury to people or property resulting from any ideas, methods, instructions or products referred to in the content.